



Analysis of existence state and deterioration mechanism of coke in a blast furnace hearth

Wen-quan Niu¹ · Jing-song Wang¹ · Guang Wang¹ · Hai-bin Zuo¹ · Xue-feng She¹ · Qing-guo Xue¹

Received: 29 March 2024 / Revised: 25 June 2024 / Accepted: 6 July 2024
© China Iron and Steel Research Institute Group Co., Ltd. 2024

Abstract

Pursuing green, low-carbon ironmaking technology primarily aims to reduce fuel ratios, especially coke ratios. Simultaneously, the reduction in coke ratios causes the coke layer in the blast furnace (BF) to become thinner, deteriorating the gas and liquid permeability of the burden column. This exacerbates coke degradation, significantly impacting the smelting process and increasing the demand for high-quality coke. To investigate the existence state of coke in the hearth, a 2500 m³ BF in China was taken as the research object, and three sets of samples at different heights of the hearth were obtained during planned outage. The results indicate that coke undergoes a significant degradation upon reaching the hearth. The proportion of coke particles smaller than 50 mm ranges from 81.22% to 89.50%. The proportion of coke particles larger than 20 mm decreases as the distance from the centerline of the tuyere increases, while the proportion of particles smaller than 10 mm increases with this distance. Additionally, the closer the bottom of the furnace is, the smaller the coke particle size becomes. The composition of slag filling the coke pores is similar to that of the final slag in the blast furnace, and the graphitization of coke is comparable to that of the final slag. The graphitization of coke starts from the surface of coke and leads to the formation of coke fines, and the graphitization degree of – 74 μm coke fines is the highest. The temperature has an effect on the reaction rate of coke solution loss, and the higher the temperature is, the faster the reaction rate is.

Keywords Blast furnace · Hearth · Coke · Graphitization · Dissolution reaction

1 Introduction

Over the past 10 years, the steel industry has grown rapidly, and China leads the world in steel production [1, 2]. Blast furnace (BF) ironmaking continues to dominate the ironmaking industry, comprising approximately 70% of the global market share. While the adoption of innovative BF ironmaking technologies helps reduce coke and coal consumption, it is not possible to completely replace coke with alternative reducing agents [3, 4]. Coke can be used as a reducing agent for iron ore, a heat source for the BF, a skeleton of the stock column, and a carbonizer for molten iron [5–7]. The evolution of coke in the BF is a

gradual and continuous process, charging from the top of the BF and undergoing multiphase reactions when it reaches the hearth, where severe degradation occurs and a large amount of coke fine is produced. Currently, the hearth is one of the key areas limiting the life of the BF [8–10]. Coke is the only material in the hearth that remains solid, and its porous structure provides an important channel for slag and iron to drip from the hearth and for air to rise [11]. The deterioration of air and liquid permeability in the hearth impedes the dripping of liquid slag and iron, causing them to adhere to the coke surface and increasing the deadman volume. This affects the smooth operation of the BF, leading to issues such as burden suspension and problematic slag discharge, and ultimately resulting in various malfunctions [12]. The coke, slag, and molten iron in the hearth always interact with each other, and their behaviors and products have a great influence on the stability of the BF and the fuel consumption per ton of iron. Only grasping the morphology and structure of coke and its accompanying substances in the hearth can improve the

✉ Jing-song Wang
wangjingsong@ustb.edu.cn

✉ Guang Wang
wangguang@ustb.edu.cn

¹ State Key Laboratory of Advanced Metallurgy, University of Science and Technology Beijing, Beijing 100083, China

efficiency of the utilization of fuel [13]. Currently, the most effective means to study the coke state of the hearth is to dissect the BF by stopping the furnace, which can directly reflect the most real state of the physical phase inside the hearth. Coke behavior and process parameters related to the BF process have been investigated through different research projects over the last years, and it has been found that the degradation process of coke mainly consists of graphitization and gasification dissolution. Due to the intricate nature of reactions occurring at high temperatures and pressures, obtaining representative coke samples from operational furnaces has traditionally been challenging. However, recent advancements in tuyere core drilling technology have facilitated efficient extraction of coke samples from active blast furnaces, offering a potentially valuable source of information on various crucial phenomena under operating conditions [9, 14–18]. Zhang et al. [19] found that the samples inside the residual iron were mainly composed of Fe and C elements, while the samples around the cold side have more complex phases including Ti_3N_2 , KAlSi_2O_6 , and Al_2O_3 . The density, graphitization degree, and thermal diffusivity have changed greatly, which is related to the existence of complex phase and the function of cooling system. Ma et al. [20] proposed that the reduction in slag basicity and the precipitation of solid CaS particles resulting from slag iron desulfurization are significant factors contributing to the deterioration of slag phase fluidity. The presence of titanium nitride (Ti_3N_4) clusters at the mineral layer–iron interface can facilitate the formation of a titanium-rich layer within the hearth. In this paper, we examine a 2500 m³ BF from a Chinese steel plant. During a planned outage, we obtained three groups of coke samples from various heights in the hearth and analyzed them. This analysis revealed the state of coke and its graphitization pattern. Laboratory experiments further investigated the graphitization and gasification reactions of coke. Our research offers detailed spatial analysis of coke degradation in blast furnaces, showing over 50% reduction in average coke size and particle distribution changes relative to the tuyere centerline and furnace depth, which is crucial for optimizing operations. We also identify specific silicates and oxides in coke pores that cause structural disintegration, linking microstructural interactions with macroscopic patterns, and addressing literature gaps. Additionally, we examine the role of temperature in coke graphitization, providing insights for enhancing coke performance. These contributions offer practical solutions for improving metallurgical processes.

Table 1 BF parameters and operating parameters

Parameter	Value	Parameter	Value
Effective volume/m ³	2500	Blast temperature/°C	1200
Hearth diameter/m	11	Coke ratio/(kg t ⁻¹)	360
Hearth height/m	4.2	Coal ratio/(kg t ⁻¹)	160
Tuyere centerline/m	14.6	Iron output/(t m ⁻³)	9220
Taphole centerline/m	10.4	Slag ratio/(kg t ⁻¹)	360

2 Materials and methods

2.1 Overview of BF and sample acquisition

A 2500 m³ BF was selected for this study. The furnace began operations in February 2008 and was decommissioned by introducing nitrogen (N₂) in June 2023, marking a total operational period of 15 years and 4 months. This BF was noted for its efficiency and longevity. It was equipped with three tap holes and 30 tuyeres, maintaining an average annual utilization factor of 2.0 t/(d m³). Detailed configuration and operating parameters are provided in Table 1.

After the blast furnace had rested and cooled down, the hearth was dissected, and samples were excavated layer by layer using an excavator. Coke samples were collected with a shovel at each predetermined depth. The sampling positions were 1 m (V-1), 1.8 m (V-2), and 2.6 m (V-3) from the centerline of the tuyere, as shown in Fig. 1. The coke and accompanying samples from different locations in the hearth were classified after being dried at 105 °C for 10 h. Slag, often combined with iron, was separated manually using magnetic separation due to the absence of a standardized method.

After slag–iron separation, the coke samples were sieved sequentially using standard sieves with sizes of 50, 20, 10, 3.2, 0.3, and 0.074 mm. The masses of coke within each size range were weighed, and the corresponding ratios were calculated under the same conditions. The macroscopic morphology of the samples, the magnetic separation process, and the sieving results are illustrated in Fig. 2.

2.2 Coke matrix heat treatment experiment

Heat treatment experiments of coke were conducted using a tube furnace with programmable temperature control (Fig. 3). The industrial analysis of the feed coke from an ironworks is provided in Table 2. The feed coke was

manually crushed and sieved to obtain particles sized 6–8 mm. Approximately 5 g of the sample was placed in a corundum crucible and inserted into the non-thermostatic zone of the furnace. The setup procedure was as follows: for temperatures below 900 °C, the heating rate was controlled at 8 °C/min; for temperatures above 900 °C, the heating rate was adjusted to 5 °C/min. Throughout the experiment, argon was used to maintain an inert atmosphere at a flow rate of 2 L/min [21–23]. In the belly area of the BF, under the influence of high temperatures

(exceeding 1200 °C), amorphous carbon gradually transforms into an orderly arrangement of graphitic carbon crystals, marking the onset of the graphitization process [24]. In conjunction with the coking temperature of the feed coke, the samples were heat-treated at three temperatures: 1373, 1573, and 1773 K. Once the furnace reached the target temperature, the coke samples were moved to the thermostatic zone and held there for half an hour. After this period, the samples were returned to the non-thermostatic zone of the furnace. The microcrystalline structure of the coke matrix samples was then analyzed using an X-ray diffractometer.

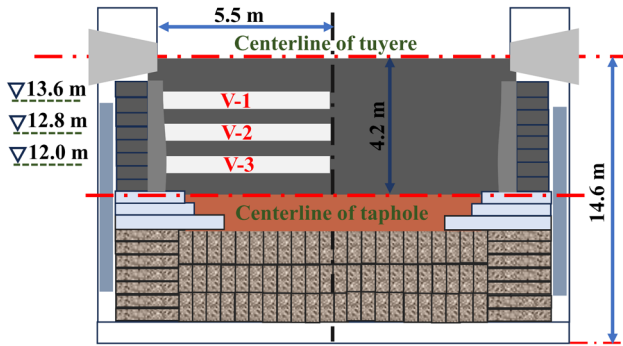


Fig. 1 Schematic diagram of hearth sampling position

2.3 Coke matrix dissolution reaction experiment

2.3.1 Low-temperature dissolution reaction

A 20 mg sample of coke matrix with particle size of -0.074 mm was placed in a thermogravimetric analyzer (HCT-4). The reaction was carried out by introducing CO₂ gas, gradually increasing the temperature to 1100 °C, and holding at this temperature for 30 min, and then, the mass loss was determined. The heating and aeration regimes are shown in Table 3.

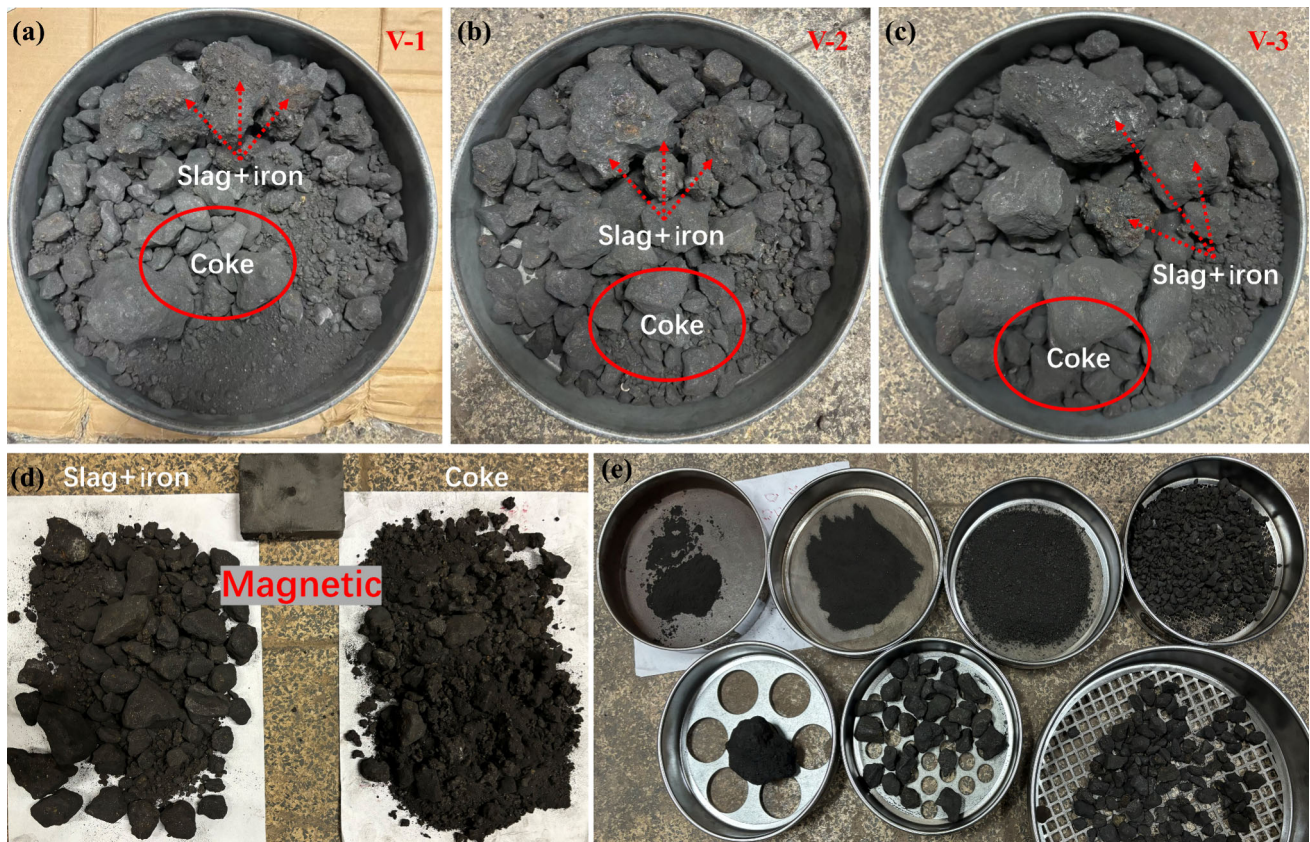


Fig. 2 Schematic diagrams of samples at different heights of hearth. **a** V-1 sample morphology; **b** V-2 sample morphology; **c** V-3 sample morphology; **d** manual magnetic separation analysis; **e** coke sample sieving

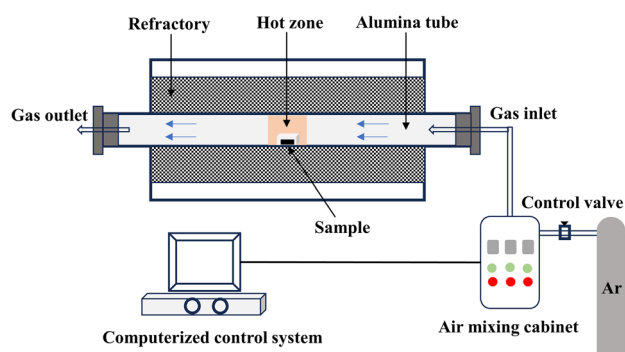


Fig. 3 Schematic diagram of horizontal tube furnace for heat treatment of feed coke

Table 2 Results of industrial analysis of feed coke (%)

Fixed carbon	Volatile matter	Ash	Moisture
80.5	2.75	14.73	1.27

Table 3 Heating and aeration regimes for low-temperature dissolution reactions

Temperature/ °C	Heating rate/ (°C min ⁻¹)	Holding time/min	Gas composition	Flux/ (mL min ⁻¹)
25–1100	20	0	CO ₂	30
1100	0	30	CO ₂	30

Table 4 Heating and aeration regimes for high-temperature dissolution reaction

Temperature/ °C	Heating rate/ (°C min ⁻¹)	Holding time/min	Gas composition	Flux/ (mL min ⁻¹)
25–1100	20	0	N ₂	30
1100–1250	5	0	CO ₂	30

2.3.2 High-temperature dissolution reaction

A 20 mg sample of coke matrix with particle size of -0.074 mm was placed in a thermogravimetric analyzer, and the temperature was increased under the N₂ atmosphere. When the temperature was increased to 1100 °C, the N₂ was replaced by the CO₂; under the CO₂ atmosphere, the gasification reaction between the coke matrix and the CO₂ took place, and the temperature was continuously increased to 1250 °C. The heating and aeration regimes are shown in Table 4.

2.4 Methods of analysis

Since coke samples within the same particle size range exhibit similar properties, this paper uses V-2 sample as an example to illustrate the state of the feed coke once it reaches the hearth. It is generally accepted that coke particles larger than 20 mm do not react violently, while particles smaller than 10 mm do. To prepare the samples, the $+20$ mm and -10 mm coke particles were fixed using epoxy resin, then ground and polished. For the preparation of powder samples, conductive adhesive tapes were attached to the sample holders, onto which coke powder was evenly sprinkled. Unadhered powders were blown away with a wash ball. After drying, the surface of the coke samples was coated with gold. The samples were then scanned using an FEI Quanta 250 scanning electron microscope (SEM) equipped with an energy dispersive spectrometer (EDS) to analyze the morphology and structure of the coke.

Additionally, selected coke samples were ground to a fine powder (-0.074 mm) using an agate mortar and pestle for X-ray diffraction (XRD) analysis (Cu K α , XRD Ultima IV, Rigaku, Japan). The scanning was performed over an angle range of 10°–90° (2θ), with a step size of 0.02° per step and a scanning speed of 10° per minute. The XRD spectra were collected by recording the scattering intensity of the coke samples. In the XRD spectra, the (002) peak is a representative feature of the carbon structure, typically observed in the 2θ range of 20°–30°. The characteristics of the (002) peak are used to assess the degree of graphitization of the coke, with narrower and sharper (002) peaks indicating a higher degree of graphitization [25, 26]. The analysis of this peak based on the Scherrer's formula and Bragg's equation for various parameters related to the carbon structure, including the stacking height L_c , the number of graphite layers n_{ave} , and the average spacing of the crystalline layers d_{002} , can be calculated as follows [23, 27]:

$$L_c = \frac{K\lambda}{\beta \cos \theta_{002}} \quad (1)$$

$$d_{002} = \frac{\lambda}{2 \sin \theta_{002}} \quad (2)$$

$$n_{ave} = \frac{L_c}{d_{002}} \quad (3)$$

where K is a constant for a given reflection plane ($K = 0.89$ for L_{002} and $K = 1.84$ for L_{100}); λ is the wavelength of X-rays, taken as 0.15418 nm; β is the half-height width; and θ_{002} is the diffraction angle of the (002) peak, (°). 0.3440 is the layer spacing of completely ungraphitized carbon. The relative difference between the calculated graphite layer spacing d_{002} and the layer spacing of ideal graphite

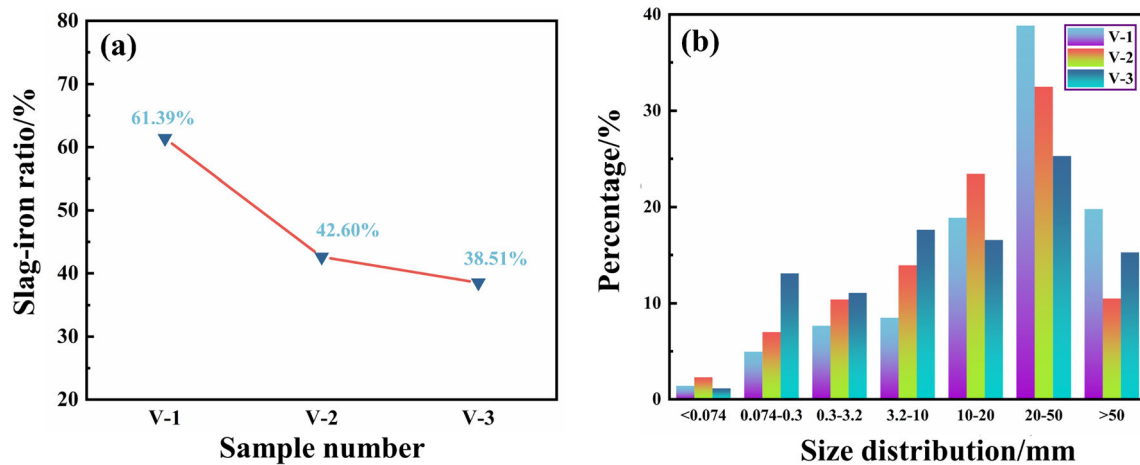


Fig. 4 Evolution of slag-iron ratio and size distribution in different hearth heights

(0.3354) is used to indicate the degree of graphitization g of the coke.

3 Results and discussion

3.1 Samples distribution characteristics in hearth

The powder generated from the sampling process and the loss from the manual slag-iron separation process was negligible compared to the total mass of the samples taken. After slag-iron separation, the coke samples were sieved and the slag-iron ratio and particle size distributions at different hearth locations were calculated and are shown in Fig. 4. The results clearly show that the slag-iron ratio in the hearth samples decreases with increasing the distance from the centerline of the tuyere (Fig. 4a). Zhu et al. [28] found that the slag-iron ratio increased continuously when the distance from the tuyere was less than 2.5 m, while the slag-iron ratio remained relatively constant or continued to increase when the distance from the tuyere was greater than 2.5 m by analyzing the slag-iron ratio of two large BF tuyere samples from a steel plant. Li et al. [29] obtained two batches of coke samples by drilling holes in the tuyere of a large BF with a volume greater than 5000 m³ and found that the slag-iron ratio increased with increasing the distance from the tuyere.

Figure 4b illustrates the particle size distribution of coke samples from various heights within the hearth. It is known that the average particle size of the feed coke in this BF is larger than 53.50 mm. However, most of the coke in the hearth has a particle size of less than 50 mm, accounting for 81.22%–89.5% of the total. Only a small portion of the coke samples (< 20%) have a particle size greater than 50 mm, and the proportion of coke smaller than 20 mm

increases significantly. This indicates that although the feed coke has a particle size significantly larger than 50 mm, once it reaches the hearth, significant degradation has occurred due to chemical reactions, thermal annealing, and other chemical and physical effects within the furnace.

The amount of coke in the 20–50 mm range decreases with increasing the distance from the centerline of the tuyere, while the amounts in the range of 3.2–10, 0.3–3.2, and 0.074–0.3 mm increase with this distance. The quantity of coke powder smaller than 0.074 mm shows no obvious change due to its small proportion and the presence of slag and metal, meaning the actual mass of coke powder in the hearth may be lower than that considered in this study.

The quantity of coke smaller than 50 mm increases gradually across different sample groups, reaching a maximum in the 20–50 mm range. According to calculations, the average coke size is 26.98 mm at the top of the hearth (V-1), 21.22 mm in the middle (V-2), and 20.30 mm at the bottom (V-3). This indicates that the closer to the bottom of the furnace, the smaller the coke particle size, showing more severe erosion by molten iron and slag. After descending to the hearth, the average size of coke particles is reduced by more than 50%.

3.2 Morphological characteristics of hearth coke

3.2.1 Morphology and state of hearth coke larger than 20 mm

The morphology of the + 20 mm coke sample was analyzed in detail using SEM and EDS scanning, as shown in Fig. 5. The microstructural image of the large-grained coke reveals a porous structure, indicating deterioration and the development of a pore structure as the coke reaches the hearth. Multiple small pores have connected to form larger

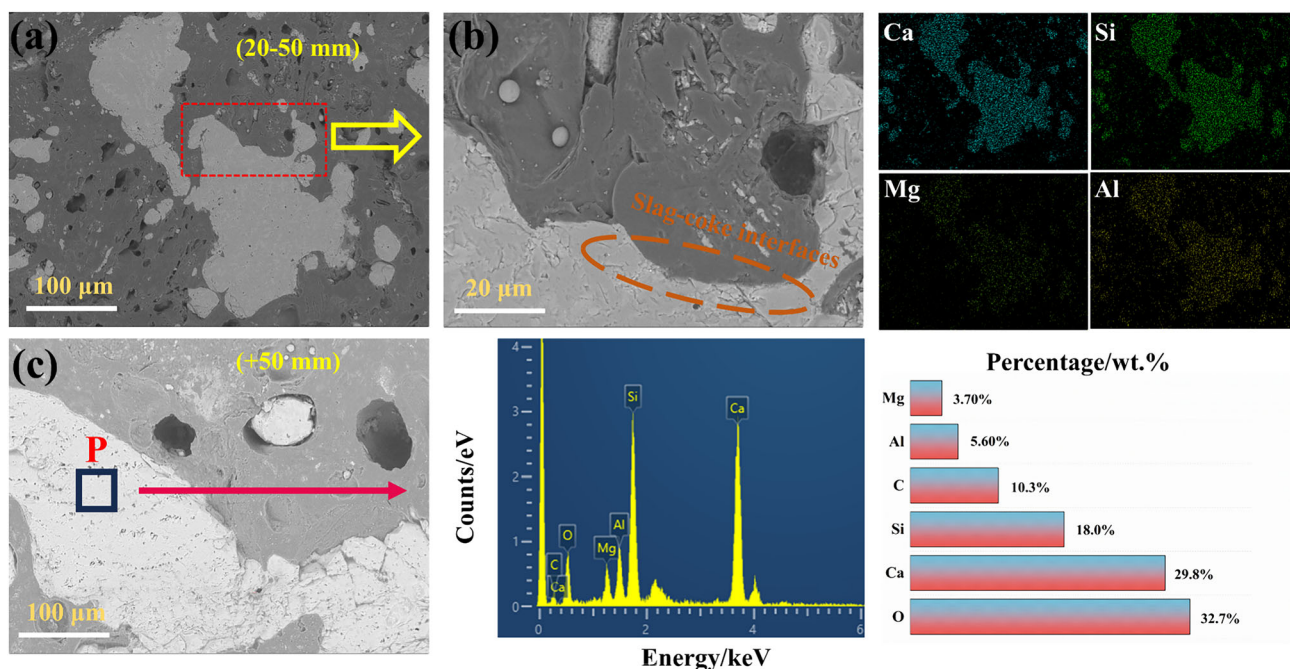


Fig. 5 SEM and EDS images of +20 mm coke samples in hearth

pores. As the pore size of the coke increases, blast furnace melts (such as slag, molten iron, or unburned pulverized coal) can migrate into the coke matrix through these connected openings (Fig. 5), filling the pores and forming a distinct slag-coke interface.

Surface scanning in Fig. 5a was performed using EDS to qualitatively analyze the composition of the slag. It was found that the slag mainly contained oxides of calcium, silicon, magnesium, and aluminum, with very few oxides of iron and alkali metals. The composition of the slag was quantitatively analyzed through point scanning of Fig. 5c by EDS, confirming that the slag composition was similar to that of the final slag. This slag was primarily composed of acidic oxides (SiO_2 and Al_2O_3) and alkaline oxides (CaO and MgO). Similar phenomena have been observed in recent studies of tuyere and hearth coke [29, 30], showing that the migration of slag to the coke matrix in the high-temperature zone of the BF is a common phenomenon; the slag in the coke pores will enter into the iron of the hearth, which affects the dissolution of coke in the iron and thus reduces the strength of the refractory material at the bottom of the furnace.

3.2.2 Morphology and state of hearth coke less than 10 mm

The morphology of coke samples with particle sizes in the range of 3.2–10 mm was analyzed by SEM and EDS, as shown in Fig. 6. The SEM images showed that the coke

had undergone severe deterioration and the stomata were highly developed; the walls of the stomata (matrix structure) were thinned, and a number of small pores were linked together to form large pores.

Figure 6a illustrates that the surface of most coke particles is extremely irregular. Compared to the feed coke, the open pores are largely filled with slag. Due to the strong reaction between the slag within the pores and the coke, the pore area of the coke in the hearth has significantly increased. This process causes the pores to gradually enlarge and swell, eventually forming large open pores, which leads to further degradation of the coke [31]. The pore structure provided an opportunity for slag to penetrate into the coke, as shown in the enlarged view of the coke particles in Fig. 6b. Surface scanning of the enlarged coke surface by EDS (Fig. 6c) revealed the presence of components such as silicates ($\text{Ca}_2\text{Al}_2\text{SiO}_7$, $\text{Ca}_2\text{MgSi}_2\text{O}_7$) and MgAl_2O_4 within the pores of the coke. This penetration led to the expansion of the internal volume and localized disintegration of the structure. The resulting cracks and debris further affected the physical and chemical properties of the coke [28]. In summary, the aggregation of slag and other substances in the pores of the coke and the destruction of the coke structural strength together led to the fragmentation, degradation, and disappearance of the coke in the hearth [32]. At the same time, due to the liquid state of slag and molten iron in the high-temperature zone of the BF, iron and slag powders are formed during the cooling process of the extracted samples. Coke powders are produced

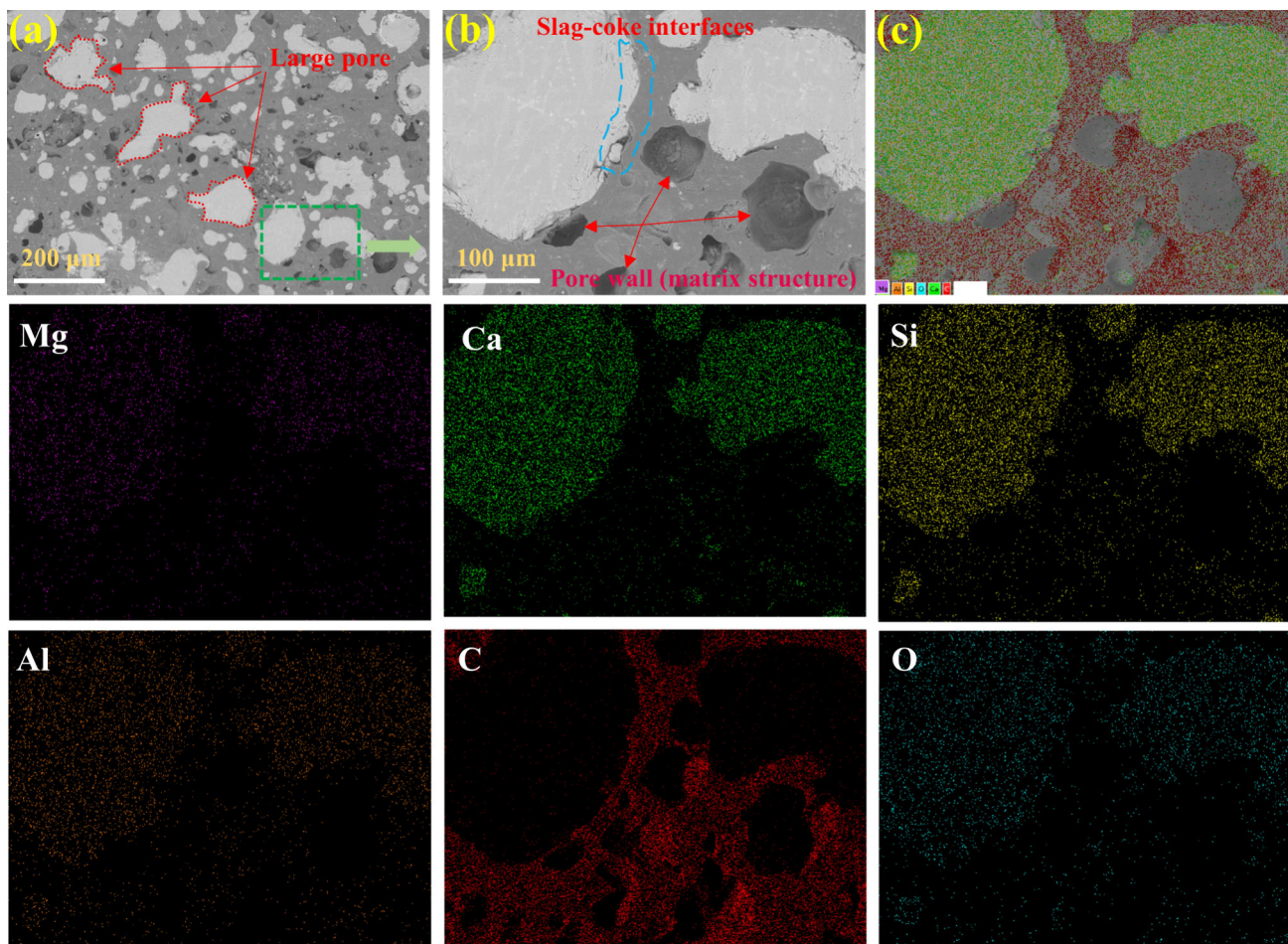


Fig. 6 SEM and EDS images of coke samples with size ranging from 3.2 to 10 mm

by a combination of factors, including chemical reactions, mechanical wear, and thermal stress. These powders can deteriorate the permeability of the deadman [30].

3.3 Graphitization of coke

X-ray diffraction is commonly used to analyze the structure of coke. Previous studies [21, 23, 29] have shown that the (002) carbon peaks can represent the structure of coke, and the 2θ of the (002) peak is in the range of 20° – 30° . The XRD patterns of the feed coke and cokes after heat treatment at 1373, 1573, and 1773 K are shown in Fig. 7. The broad peaks in the range of 10° – 90° represent the (002) peaks of carbon microcrystals of the coke, and the sharp peaks at around 26° are SiO_2 peaks. The broad and dispersed diffraction peaks indicate lower carbon microcrystalline stacking height values and suggest a poorly ordered carbon structure. As the temperature increased from 1373 to 1773 K, the (002) carbon peaks became narrower and more prominent, indicating an increase in the orderliness of the carbon structure.

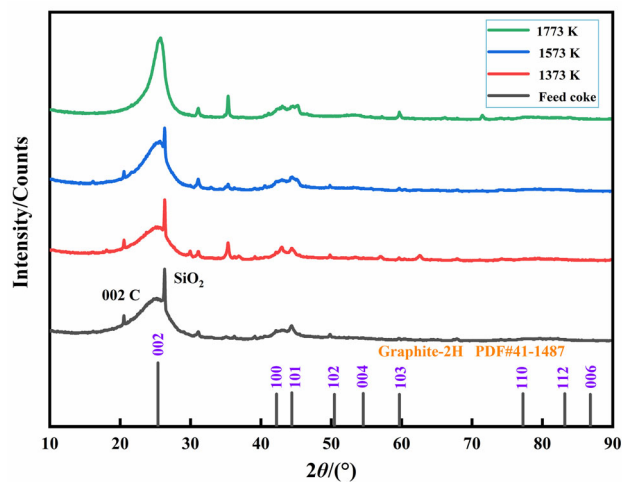
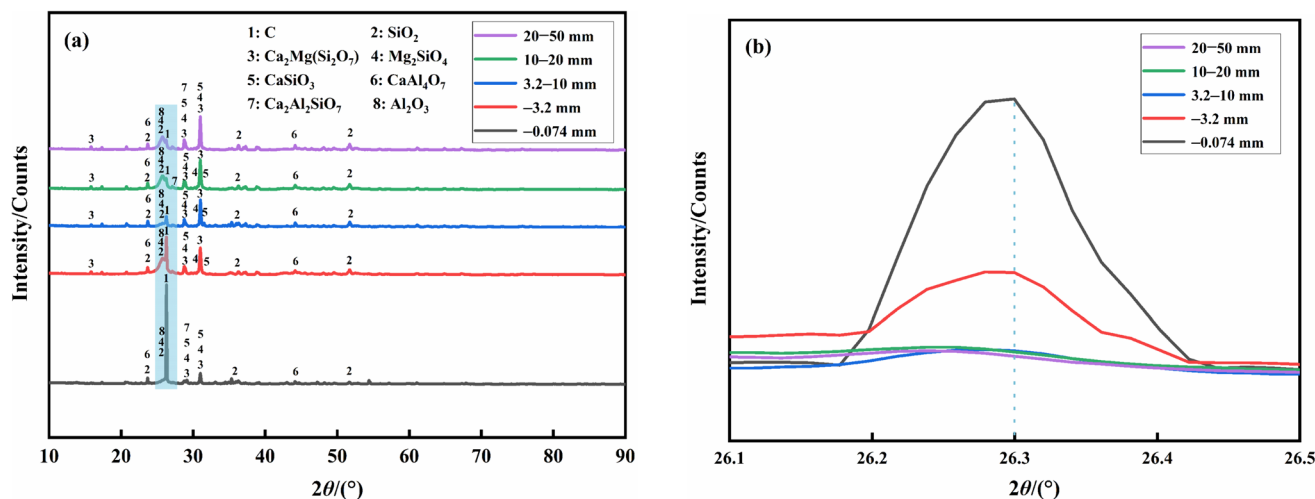


Fig. 7 XRD patterns of coke after heat treatment at 1373, 1573, and 1773 K

The characteristic SiO_2 peaks gradually disappeared, which was attributed to the carbothermal reduction of SiO_2 . Temperature is one of the key factors affecting the

Table 5 Structural parameters of coke at different temperatures

Coke	$\theta_{002}/(^{\circ})$	d_{002}/nm	$\beta/(^{\circ})$	L_c/nm	n_{ave}
Feed coke	25.116	0.3546	4.133	1.948	6
1373 K	25.443	0.3501	3.413	2.360	7
1573 K	25.629	0.3476	3.018	2.670	8
1773 K	25.748	0.3460	2.351	3.428	10

**Fig. 8** XRD patterns of coke with different sizes in hearth

graphitization of coke. The diffraction pattern of coke at various temperatures was analyzed using XRD analysis software to obtain the diffraction angle and half-height width of the coke peaks. The three characteristic values of the microcrystalline structure of coke were then calculated using Eqs. (1)–(3). As shown in Table 5, as the temperature increases, d_{002} and β decrease, while L_c and n_{ave} increase, indicating that the graphitization of the coke gradually deepens.

XRD analyses were carried out on different grain sizes of the hearth coke to study the evolution of its structure, as shown in Fig. 8. The structural parameters of the hearth coke with different grain sizes are presented in Table 6. The graphite (002) peak is the most dominant in the XRD patterns of the coke, indicating that the dominant internal structure is a graphite-like carbon structure. Minerals are also labeled in the XRD patterns (Fig. 8a). It was found that the smaller the coke particle size, the narrower the (002) peak (Fig. 8b), indicating a more ordered carbon structure.

Compared with the feed coke, the hearth coke shows a distinctive mineral composition, primarily consisting of $\text{Ca}_2\text{Mg}(\text{Si}_2\text{O}_7)$, $\text{Ca}_2\text{Al}_2\text{SiO}_7$, MgAl_2O_4 , and CaSiO_3 . As the coke particle size decreases, the characteristic peaks of minerals become less pronounced. The values of d_{002} and β

decrease, while L_c increases from 7.281 to 10.703 nm, and n_{ave} increases from 21 to 32 layers. This indicates that the degree of graphitization of the coke is gradually increasing. The -0.074 mm coke powder exhibits the highest degree of graphitization, likely due to smaller coke particles being more easily catalyzed by temperature, alkali metals, and metallic iron, leading to a significant increase in graphitization.

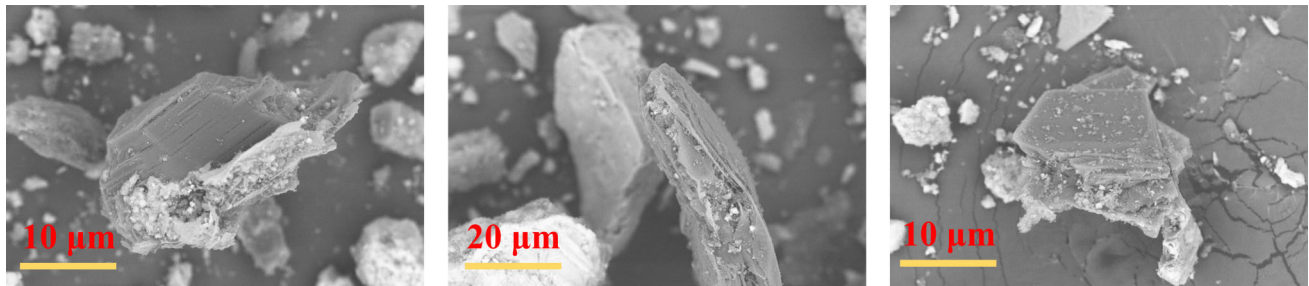
Recent studies have constructed a relationship between L_c values and temperature as shown in Eq. (4) [23, 33–35]. The stacking height of the carbon lattice surface is proportional to the temperature T . The larger the L_c value, the more stable the carbon structure, and the higher the degree of graphitization [31].

$$L_c = 0.00443T - 1.79694 \quad (4)$$

SEM images of -0.074 mm coke powders at high magnification clearly reveal their graphitic properties (Fig. 9). Undeveloped hexagonal prismatic and lamellar graphite crystals and their combinations were observed in the -0.074 mm coke powder. Gupta et al. [21] and Li et al. [30] observed that graphitization of coke in the high-temperature region starts from the coke surface and leads to the formation of coke fines; the highly graphitized coke surface catalyzed by iron is washed away. During

Table 6 Structural parameters of coke with different grain sizes in hearth

Size range/mm	$\theta_{002}/(^{\circ})$	d_{002}/nm	$\beta/(^{\circ})$	L_c/nm	n_{ave}
20–50	26.217	0.3399	1.108	7.281	21
10–20	26.234	0.3397	0.952	8.474	25
3.2–10	26.248	0.3395	0.916	8.807	26
0.3–3.2	26.281	0.3391	0.881	9.158	27
– 0.074	26.381	0.3378	0.754	10.703	32

**Fig. 9** SEM image of graphite crystals observed in – 0.074 mm coke powder

graphitization, the ash of coke migrates from the interior to the surface under thermal stress and then volatilizes [36, 37].

3.4 Analysis of coke dissolution reaction

The coke reactivity index (CRI) is an index used to evaluate the ability of the coke matrix to react with CO_2 at 1100 °C. Generally, coke with higher reactivity is considered to have a poorer ability to resist CO_2 erosion. Figure 10 shows the reaction curves of coke and CO_2 at different temperature intervals. It can be seen that when the temperature is below 900 °C, the coke mass loss curves are quite similar, indicating that the mass loss reaction has not yet started. The reaction initiation temperature is defined as the temperature at which the mass loss rate reaches 2.5% [38]. With the increase in temperature, the solution loss reaction gradually intensifies, leading to a larger disparity in the solution loss rate. This indicates that the influence of temperature on the solution loss rate of coke during the pre-reaction period is minimal. The mass reduction of coke in this period includes not only the amount lost through the gasification reaction but also the volatile matter rapidly precipitated from the coke due to the high-temperature CO_2 flow passing through it.

Figure 10a shows the reaction curve of coke and CO_2 at 25–1100 °C. When the temperature reaches 957 °C, the mass loss reaction starts, with the reaction rate first gradually increasing and then gradually decreasing to zero. The final mass loss rate is 84.90%. Figure 10b shows the reaction curve of coke and CO_2 at temperatures of

1100–1250 °C. Before CO_2 was introduced, the mass loss of coke did not change significantly. After CO_2 was introduced, the reaction rate increased sharply, more rapidly than in the former case. As the temperature increased, the reaction rate gradually decreased to zero, with the final mass loss rate being 85.28%.

Since the coke was ground into fine particles, the gasification nature of the coke matrix played a major role. By comparing the reaction curves at different temperature intervals, it was found that temperature is also an important factor affecting the mass loss reaction rate. Higher temperatures resulted in faster reaction rates; however, there was little difference in the final mass loss rate.

4 Conclusions

1. The coke is severely degraded upon reaching the hearth, with the average size decreasing by more than 50%. The proportion of + 20 mm coke decreases as the distance from the tuyere centerline increases, while the proportion of –10 mm coke increases with the distance. Closer to the bottom of the furnace, the coke size is smaller, and it is more easily attacked by molten iron and slag.
2. The slag composition of the coke pores is similar to that of the BF final slag, which mainly consists of acidic oxides (SiO_2 and Al_2O_3) and basic oxides (CaO and MgO); components such as silicates ($\text{Ca}_2\text{Al}_2\text{SiO}_7$, $\text{Ca}_2\text{MgSi}_2\text{O}_7$) and MgAl_2O_4 were found in the coke pores, which led to the expansion of the internal

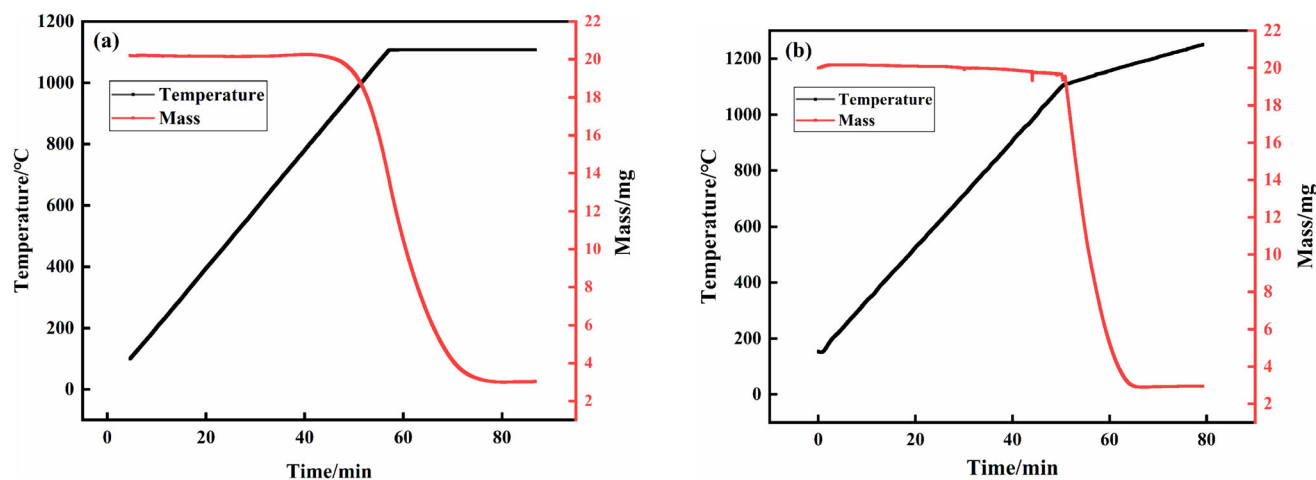


Fig. 10 Dissolution reaction of coke matrix at different temperature intervals

volume and the disintegration of the structure of the local area.

- Higher temperatures increase the degree of coke graphitization. The -0.074 mm coke powder shows the smallest d_{002} value, the largest L_c value, and the highest graphitization degree. High-magnification SEM reveals undeveloped graphite crystals in the -0.074 mm coke powder.
- Temperature is also one of the important factors affecting the coke dissolution reaction. The higher the temperature, the faster the reaction rate; however, there is little difference in the final dissolution rate.

Acknowledgements This work was supported by the National Natural Science Foundation of China (Grant No. U1960205), China Baowu Low Carbon Metallurgy Innovation Foundation (Grant Nos. BWLCF202101 and BWLCF202104), and China Minmetals Science and Technology Special Plan Foundation (Grant No. 2020ZXA01).

Declarations

Conflict of interest Guang Wang is a youth editorial board member for *Journal of Iron and Steel Research International* and was not involved in the editorial review or the decision to publish this article. The authors declare that they have no known competing financial interests or personal relationships that could have appeared to influence the work reported in this paper.

References

- W. Zhang, W.Y. Dai, J. Iron Steel Res. Int. 31 (2024) 1320–1343.
- T.T. Zhang, J. Ding, B.Y. Ma, Z.L. Liu, C. Yu, C.J. Deng, J. Iron Steel Res. Int. 31 (2024) 1291–1303.
- B. Rahmatmand, A. Tahmasebi, H. Lomas, T. Honeyands, P. Koshy, K. Hockings, A. Jayasekara, Fuel 336 (2023) 127077.
- W. Zhang, J. Dai, C.Z. Li, X.B. Yu, Z.L. Xue, H. Saxén, Steel Res. Int. 92 (2021) 2000326.
- K.J. Li, R. Khanna, J.L. Zhang, Z.J. Liu, V. Sahajwalla, T.J. Yang, D.W. Kong, Fuel 133 (2014) 194–215.
- H. Lomas, R. Roest, S. Gupta, R.A. Pearson, R. Fetscher, D.R. Jenkins, R. Pearce, R. Kanniala, M.R. Mahoney, Fuel 200 (2017) 89–99.
- Z.Y. Chang, J.L. Zhang, X.J. Ning, Fuel 253 (2019) 32–39.
- Y.Y. Cui, B. Yang, K. Zhong, J.N. Shao, China Metallurgy 32 (2022) No. 3, 73–79.
- Q. Niu, Study on the influencing factors of long-life BF hearth bottom, University of Science and Technology Beijing, Beijing, China, 2020.
- X.S. Zhang, Y. Zhang, J. Sun, G.L. Jia, M.X. Zhao, China Metall. 31 (2021) No. 11, 9–15.
- H.B. Zhu, W.L. Zhan, Z.J. He, Y.C. Yu, Q.H. Pang, J.H. Zhang, Int. J. Miner. Metall. Mater. 27 (2020) 1226–1233.
- X.B. Wang, J.G. Wang, D. Liang, S. Meng, K.X. Jiao, J.L. Zhang, Iron and Steel 58 (2023) No. 12, 31–40.
- A.L. Chaika, V.V. Lebed, B.V. Kornilov, A.A. Moskalina, S.A. Karikov, Steel Transl. 51 (2021) 68–72.
- R.R. Willmers, Metall. Res. Technol. 89 (1992) 241–250.
- O. Kerkkonen, in: J.M. Emling, E.C. Williams (Eds.), Iron & Steel Technol. Conf. Proc., Curran Associates, Inc., Cleveland, 2004, pp. 469–481.
- S. Dong, N. Paterson, S.G. Kazarian, D.R. Dugwell, R. Kandiyoti, Energy Fuels 21 (2007) 3446–3454.
- R. Kanniala, O. Kerkkonen(2007), in: J.M. Emling, E.C. Williams (Eds.), Iron & Steel Technol. Conf. Proc., Curran Associates, Inc., Indianapolis, pp. 111–120
- W.J. Zhang, T. Shi, Q.F. Zhang, Y.P. Cao, H. Qian, X.C. Wu, J. Li, Q. Zhang, G.Z. Yang, J.H. Yang, Fuel 251 (2019) 218–223.
- L. Zhang, J.L. Zhang, K.X. Jiao, C. Wang, ISIJ Int. 60 (2020) 1655–1661.
- H.B. Ma, K.X. Jiao, J.L. Zhang, X.Y. Fan, Y.B. Zong, J. Sustain. Metall. 8 (2022) 1662–1674.
- S. Gupta, Z.Z. Ye, R. Kanniala, O. Kerkkonen, V. Sahajwalla, Fuel 113 (2013) 77–85.
- M. Lundgren, R. Khanna, L.S. Ökvist, V. Sahajwalla, B. Björkman, Metall. Mater. Trans. B 45 (2014) 603–616.
- Z.Y. Guo, Y.B. Zong, J.L. Zhang, Z.X. Xiao, Y.X. Liu, Z. Xu, K.X. Jiao, Fuel 359 (2024) 130492.
- W.L. Zhan, C. Sun, Y.C. Yu, Q.H. Pang, J.H. Zhang, Z.J. He, Chin. J. Eng. 40 (2018) 690–696.
- Y. Hishiyama, M. Nakamura, Carbon 33 (1995) 1399–1403.
- L. Lu, V. Sahajwalla, C. Kong, D. Harris, Carbon 39 (2001) 1821–1833.

- [27] Q. Niu, S. Cheng, W. Xu, W. Niu, A. Li, H. Ma, S. Zhang, T. Cao, *ISIJ Int.* 58 (2018) 667–676.
- [28] W.C. Zhu, W.D. Zhang, D.Q. Wang, H.S. Zhang, H.B. Shen, *Research on Iron and Steel* 42 (2014) No. 2, 9–13.
- [29] K.J. Li, J.L. Zhang, M.M. Sun, C.H. Jiang, Z.M. Wang, J.B. Zhong, Z.J. Liu, *Fuel* 225 (2018) 299–310.
- [30] K.J. Li, J.L. Zhang, Y.X. Liu, M. Barati, Z.J. Liu, J.B. Zhong, B.X. Su, M.F. Wei, G.W. Wang, T.J. Yang, *Metall. Mater. Trans. B* 47 (2016) 811–818.
- [31] Z.Y. Guo, K.X. Jiao, J.L. Zhang, H.B. Ma, S. Meng, Z.Y. Wang, J. Zhang, Y.B. Zong, *ACS Omega* 6 (2021) 25430–25439.
- [32] S. Meng, K.X. Jiao, J.L. Zhang, C. Wang, L. Zhang, Z.Y. Guo, Z.X. Xiao, *Fuel Process. Technol.* 242 (2023) 107650.
- [33] S. Dong, N. Paterson, S.G. Kazarian, D.R. Dugwell, R. Kandiyoti, *Energy Fuel* 21 (2007) 3446–3454.
- [34] S. Gupta, V. Sahajwalla, P. Chaubal, T. Youmans, *Metall. Mater. Trans. B* 36 (2005) 385–394.
- [35] M. Kawakami, H. Kanba, K. Sato, T. Takenaka, S. Gupta, R. Chandratilleke, V. Sahajwalla, *ISIJ Int.* 46 (2006) 1165–1170.
- [36] S.S. Gornostayev, J.J. Härkki, *Carbon* 45 (2007) 1145–1151.
- [37] T. Qiu, J.G. Yang, X.J. Bai, *Int. J. Miner. Metall. Mater.* 27 (2020) 162–172.
- [38] W.Z. Sun, D.S. Hu, *Baosteel Technol.* (2015) No. 6, 10–14.

Springer Nature or its licensor (e.g. a society or other partner) holds exclusive rights to this article under a publishing agreement with the author(s) or other rightsholder(s); author self-archiving of the accepted manuscript version of this article is solely governed by the terms of such publishing agreement and applicable law.